Journal of Russian Laser Research, Volume 34, Number 4, July, 2013

ABSORPTION AND SCATTERING OF LIGHT BY HYBRID METAL/J-AGGREGATE NANOPARTICLES: PLASMON–EXCITON COUPLING AND SIZE EFFECTS

Vladimir S. Lebedev[1,2]* **and Anton S. Medvedev**[1]

[1] *Moscow Institute of Physics and Technology (State University)*
Institutskiĭ per. 9, Dolgoprudnyĭ, Moscow Region 141700, Russia

[2] *P. N. Lebedev Physical Institute, Russian Academy of Sciences*
Leninskii Prospect 53, Moscow 119991, Russia

*Corresponding author e-mail: vlebedev @ sci.lebedev.ru

Abstract

We report the results of our theoretical studies of the optical properties of hybrid nanoparticles consisting of the metal core covered with molecular J-aggregates. We evaluate the cross sections of absorption and scattering of light by such particles on the basis of the extended Mie theory for two concentric spheres with material dielectric functions that take into account the size effect associated with scattering of free electrons from the core/shell interface. We carry out our calculations in a wide range of light wavelengths and geometrical parameters of the composite system for silver and gold core and for a J-aggregate shell composed of different cyanine dyes. The results obtained demonstrate the quite different behavior of the extinction spectra of such particles caused by the different strengths of interaction between the Frenkel exciton and the dipolar or multipolar plasmons. We pay particular attention to the investigation of spectral peak positions associated with the eigenfrequencies of hybrid modes in the system and peak intensities as functions of reduced oscillator strength in the molecular J-band for various relationships between the core radius and shell thickness. This provides an efficient means for the explanation of the main features in the optical properties of metal/J-aggregate nanoparticles and can be used for an effective control of the plasmon–exciton coupling strength in such hybrid complexes.

Keywords: nanophotonics, absorption and scattering of light, plasmon–exciton interaction, size-dependent effects, hybrid nanoparticles, metal/J-aggregate complexes, cyanine dye.

1. Introduction

In recent years, novel composite materials with unique optical properties have become a hot research topic because of the fundamental interest in physics and attractive potential applications in nanotechnology. Studies of the optical properties of different composite nanostructures are of considerable interest for the development of optoelectronic devices such as light-emitting diodes [1], photovoltaic cells [2], photonic switches [3, 4], and memory elements [5]. Knowledge of the optical properties of hybrid materials and understanding the effects associated with their interaction with light are necessary for many applications of nanophotonics and near-field optics [6–10], including nanolasers [11, 12].

In the past decade, a considerable amount of research has been devoted to the investigation of optical properties of various nanoparticles including pure metallic particles and metal–dielectric or metal–semiconductor composites [13–16]. The unique properties of metallic nanoparticles are well known.

Manuscript submitted by the authors in English on July 10, 2013.

Optical properties of hybrid metal-based nanoparticles have a number of specific features as compared to the case of pure metallic particles. An interesting example of the hybrid nanoparticle is the so-called metallic nanoshells [17]. Such particles consist of a thin noble metal shell (Ag or Au) and a dielectric core (SiO_2). The optical properties of metallic nanoshells have been studied in a series of works (see, review [18]).

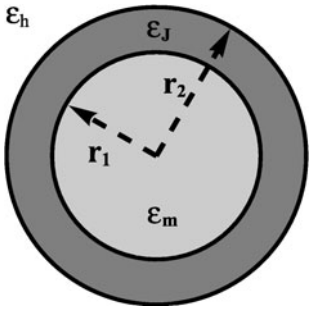

Fig. 1. Schematic structure of a spherical particle consisting of the metallic core $\varepsilon_{\rm m}$ covered with the molecular J-aggregates of cyanine dye $\varepsilon_{\rm J}$ and surrounded by a host medium with permittivity $\varepsilon_{\rm h}$.

In this work, we concentrate on the studies of optical properties of another type of hybrid nanoparticles. They consist of a metallic core coated with a J-aggregate of dye molecules (see Fig. 1). The J-aggregate exhibits sharp optical absorption, called the J-band, which is red-shifted from the monomer band, resonance fluorescence with small Stokes shift, large oscillator strength, ultrashort radiative lifetime, and remarkable nonlinear optical susceptibility leading to fast electronic response [19]. These properties are usually interpreted in terms of the Frenkel exciton delocalized over the molecular building blocks of the aggregate. Molecular J-aggregates are of special interest as photographic sensitizers, for solar photochemical energy conversion, and for nonlinear optics related to superfluorescence. In addition, they are considered as a possible organic component of various heterostructures in the development of novel optoelectronic devices.

Certain types of cyanine dyes are able to form J-aggregates in solutions, in polymer matrices, and on solid surfaces, including metal films. However, in [20] the J-aggregation of cyanine dyes on the surface of noble-metal nanoparticles in aqueous solutions was demonstrated. This opens an opportunity to study the electromagnetic coupling of an organic shell of a nanoparticle with its metallic core and, hence, to investigate the influence of the plasmon–exciton interaction on the optical properties of metal/J-aggregate complexes.

Hybrid nanoparticles consisting of a noble metal core (Ag or Au) covered with a monolayer J-aggregate of 3,3′-disulfopropyl-5,5′-dichlorothiacyanine sodium salt (TC) with overall particle diameter about 10 nm and shell thickness about 1 nm (as in [20]) were investigated in [21–27]. Experimental studies of the absorption spectra of such particles have shown their remarkable optical properties associated with the localized-surface-plasmon resonance of a core and the Frenkel exciton of a dye shell. Transmission-electron-microscopy observations revealed the spherical morphology of nanoparticles. In [22–25], the photo-initiated energy transfer in such nanostructured complexes was studied using near-field optical microscopy [23] and coherent polarization coupling between the exciton of a molecular J-aggregate and the electronic polarization of a metallic core [24]. It was demonstrated that the narrow exciton band of J-aggregates can coherently and selectively couple to the bound electronic transition dipoles in Au or to the plasmon oscillation of free electrons in Ag particles. It was also shown that the exciton spectral and temporal properties vary significantly while interacting with the metallic core compared to the case of J-aggregate monolayers on bulk-metal surfaces [22,25]. A theoretical description of the absorption spectra of Ag and Au nanoparticles covered with TC J-aggregate in aqueous solution was also made in [26,27]. The approach used in [24–27] is justified within the framework of applicability of the quasistatic approximation of the Mie theory and the simple model of dipole polarizability of two concentric spheres, i.e., when the particle size is much smaller than the wavelength of light.

In the metal/TC-dye system, the exciton resonance frequency of the J-aggregate is far from the peak of localized surface plasmon resonance so that the plasmon–exciton coupling is weak enough. However,

the coupling strength increases considerably when the plasmon- and exciton-peak positions become close to each other. The plasmon–exciton interaction in such a system was studied in [28] by measuring the light scattering spectra of single Au particles (from 70 to 130 nm diameter) coated with a J-aggregate of 1,1′-disulfopropyl-2,2′-cyanine triethylammonium salt (PIC). Spectroscopic measurements, performed using a far-field optical microscope, have shown that for such a system the surface plasmon polarization affects the peak and shape of the J-aggregate absorption band. The strong coupling between the electronic transitions of organic components [TDBC: 5, 5′, 6, 6′-tetrachloro-1-1′-diethyl-3, 3′-di(4-sulfobutyl)-benzimidazolocarbocyanine] and the plasmon modes of Au nanoparticles with different sizes surrounded with a molecular J-aggregate was experimentally studied in [29].

In this work, we present our theoretical results on optical properties of hybrid nanoparticles consisting of a metallic core and a molecular J-aggregate shell of cyanine dyes in the aqueous solution. We evaluate absorption and scattering spectra of such nanoparticles in a wide range of geometrical parameters of the composite system (core radius $5 - 65$ nm; shell thickness $1 - 5$ nm), and light wavelengths from the ultraviolet to the near-infrared region for silver and gold cores. As an organic shell, we use four anionic cyanine dyes: TC, PIC, OC (3,3′-disulfopropyl-5,5′-dichlorooxacyanine triethylammonium salt), and NK2567 (2,2′-dimethyl-8-phenyl-5,6,5′,6′-dibenzothiacarbocyanine chloride) having quite different values of the reduced oscillator strengths and for which the J-band absorption maxima are located in different wavelength regions. Our calculations are based on the extended Mie theory for absorption and scattering of light by two-component spherical particles, which is applicable for an arbitrary relationship between the overall particle radius and light wavelength. The frequency-dependent dielectric function of a metallic core is described by taking into account both contributions of the free electrons and the interband transitions. We modify the first (Drude-like) term in our calculations taking into account the size-dependent effect associated with scattering of free electrons on the surface of a metallic core. We describe the dielectric function of the J-aggregate shell using a simple model for the anharmonic oscillator with a reduced oscillator strength for the J-band transition.

One of our major goals is to demonstrate the quite different influence of the interaction between the surface plasmons localized on the metallic core of a hybrid nanoparticle with the molecular exciton in its J-aggregate shell on the behavior of the absorption and scattering spectra. The results obtained provide new data on the efficiency and features of interaction of the Frenkel exciton in a dye shell with both the dipolar and quadrupolar plasmons in a metallic core as compared to the case of molecular J-aggregates put on the bulk metal surfaces. We pay special attention to the investigation of size effects in such hybrid complexes and the demonstration of their strong influence on the optical properties of metal/J-aggregate particles.

2. Basic Expressions of the Extended Mie Theory for the Absorption and Scattering Cross Sections

For sufficiently dilute suspensions, when interparticle effects may be neglected, the behavior of the absorption and scattering spectra of hybrid spherical nanoparticles can be described on the basis of the modified Mie theory combined with a model for the field description in the concentric spheres under appropriate boundary conditions. The exact description of absorption and scattering of light by multilayered spheres has been described exactly in many papers. As a first approach, Aden and Kerker [30] and Güttler [31] have extended the Mie theory of scattering and absorption of light by a uniform spherical

particle [32] to spheres with a single external layer. The results of these works were further reproduced by several authors (e.g., [33,34]). Extension to an arbitrary number of layers was made in [35] using the matrix formalism and in [36,37] on the basis of the recursion formalism for the scattering coefficients of multilayered spherical particles. The theory developed was widely used for the determination of optical properties of different composite particles (see, [38–43] and monographs [44,45]).

A schematic view of the hybrid particle consisting of a core with radius r_1 and a shell with thickness $\ell = r_2 - r_1$ surrounded by a lossless host material with permittivity $\varepsilon_{\rm h}(\omega)$ and permeability $\mu_{\rm h} = 1$ is shown in Fig. 1. It is assumed that the concentric spheres are made of homogenous isotropic materials with frequency-dependent complex dielectric functions $\varepsilon_1(\omega)$ and $\varepsilon_2(\omega)$ and permeabilities $\mu_1 = \mu_2 = 1$. The particle is illuminated by a monochromatic plane wave $\propto \exp(-i\omega t + ik_{\rm h}z)$. The incident wave is partially scattered and absorbed by the particle. Using this approach, one can obtain general expressions for the cross sections of scattering and absorption of light by a multilayered sphere by integrating the Poynting vector over a spherical surface of large radius. They can be represented in the same form as in the case of a bare spherical particle [44]

$$\sigma_{\rm abs} = \frac{\pi}{2k_{\rm h}^2}\sum_{n=1}^{\infty}\left[(2n+1)\left(2-|2a_n+1|^2-|2b_n+1|^2\right)\right], \tag{1}$$

$$\sigma_{\rm scat} = \frac{2\pi}{k_{\rm h}^2}\sum_{n=1}^{\infty}\left[(2n+1)\left(|a_n|^2+|b_n|^2\right)\right]. \tag{2}$$

Here, a_n and b_n are the expansion coefficients of the transverse electric (TE) and transverse magnetic (TM) modes of the scattered wave, respectively, and $k_{\rm h} = \omega\sqrt{\varepsilon_{\rm h}}/c$ is the wave number of light in the host medium.

The total extinction cross section $\sigma_{\rm ext} = \sigma_{\rm abs} + \sigma_{\rm scat}$ is expressed through the complex amplitude coefficients of the scattered wave as follows:

$$\sigma_{\rm ext} = \frac{2\pi}{k_{\rm h}^2}\sum_{n=1}^{\infty}(2n+1)\,{\rm Re}\{a_n+b_n\}. \tag{3}$$

The behavior and values of the expansion coefficients a_n and b_n in Eqs. (1)–(3) are determined by the specificity of the problem. They also depend substantially on the geometrical parameters of the hybrid particle and the dielectric properties of its core, shell, and the surrounding medium.

In the case of a two-component core-shell particle (see Fig. 1), we derived the general expressions for complex expansion coefficients a_n and b_n of the scattered electromagnetic field using the theoretical approach described above and the boundary conditions for the electromagnetic fields at $r = r_1$ and $r = r_2$. For the problem considered in this paper, it is convenient to write the final formulas for a_n and b_n in the form

$$a_n = -X_n^{(a)}/Y_n^{(a)}, \qquad b_n = -X_n^{(b)}/Y_n^{(b)}, \tag{4}$$

where $X_n^{(a)}$, $Y_n^{(a)}$ and $X_n^{(b)}$, $Y_n^{(b)}$ are functions expressed in terms of determinants.

The explicit expressions for the $X_n^{(a)}$ and $Y_n^{(a)}$ functions determining the contribution of TE modes

are given by [43]

$$X_n^{(a)} = \begin{vmatrix} j_n(k_1r_1) & j_n(k_2r_1) & y_n(k_2r_1) & 0 \\ u_n'(k_1r_1) & u_n'(k_2r_1) & v_n'(k_2r_1) & 0 \\ 0 & j_n(k_2r_2) & y_n(k_2r_2) & j_n(k_{\rm h}r_2) \\ 0 & u_n'(k_2r_2) & v_n'(k_2r_2) & u_n'(k_{\rm h}r_2) \end{vmatrix}, \tag{5}$$

$$Y_n^{(a)} = \begin{vmatrix} j_n(k_1r_1) & j_n(k_2r_1) & y_n(k_2r_1) & 0 \\ u_n'(k_1r_1) & u_n'(k_2r_1) & v_n'(k_2r_1) & 0 \\ 0 & j_n(k_2r_2) & y_n(k_2r_2) & h_n^{(1)}(k_{\rm h}r_2) \\ 0 & u_n'(k_2r_2) & v_n'(k_2r_2) & w_n'(k_{\rm h}r_2) \end{vmatrix}. \tag{6}$$

Here, $k_1 = \omega\sqrt{\varepsilon_1}/c$ and $k_2 = \omega\sqrt{\varepsilon_2}/c$ are the wave numbers of light in the core and in the shell of the particle, respectively, $\varepsilon_1 \equiv \varepsilon_{\rm m}(\omega)$ and $\varepsilon_2 \equiv \varepsilon_{\rm J}(\omega)$ are the complex permittivities of the metallic core and the dye shell at the operating frequency, r_1 is the radius of the core, r_2 is the outer radius of the shell, $j_n(z)$, $y_n(z)$, and $h_n^{(1)}(z)$ are the spherical Bessel, Neumann, and Hankel functions, and $u_n(z) = zj_n(z)$, $v_n(z) = zy_n(z)$, and $w_n(z) = zh_n^{(1)}(z)$ are the spherical Riccati–Bessel, Riccati–Neumann, and Riccati–Hankel functions, respectively. The prime denotes differentiation of functions with respect to their argument.

Similarly, in the case of two-component particles the final expressions for the $X_n^{(b)}$ and $Y_n^{(b)}$ functions determining the contribution of TM-modes can be written as [43]

$$X_n^{(b)} = \begin{vmatrix} j_n(k_1r_1) & \sqrt{\varepsilon_2/\varepsilon_1}\, j_n(k_2r_1) & \sqrt{\varepsilon_2/\varepsilon_1}\, y_n(k_2r_1) & 0 \\ u_n'(k_1r_1) & \sqrt{\varepsilon_1/\varepsilon_2}\, u_n'(k_2r_1) & \sqrt{\varepsilon_1/\varepsilon_2}\, v_n'(k_2r_1) & 0 \\ 0 & \sqrt{\varepsilon_2/\varepsilon_{\rm h}}\, j_n(k_2r_2) & \sqrt{\varepsilon_2/\varepsilon_{\rm h}}\, y_n(k_2r_2) & j_n(k_{\rm h}r_2) \\ 0 & \sqrt{\varepsilon_{\rm h}/\varepsilon_2}\, u_n'(k_2r_2) & \sqrt{\varepsilon_{\rm h}/\varepsilon_2}\, v_n'(k_2r_2) & u_n'(k_{\rm h}r_2) \end{vmatrix}, \tag{7}$$

$$Y_n^{(b)} = \begin{vmatrix} j_n(k_1r_1) & \sqrt{\varepsilon_2/\varepsilon_1}\, j_n(k_2r_1) & \sqrt{\varepsilon_2/\varepsilon_1}\, y_n(k_2r_1) & 0 \\ u_n'(k_1r_1) & \sqrt{\varepsilon_1/\varepsilon_2}\, u_n'(k_2r_1) & \sqrt{\varepsilon_1/\varepsilon_2}\, v_n'(k_2r_1) & 0 \\ 0 & \sqrt{\varepsilon_2/\varepsilon_{\rm h}}\, j_n(k_2r_2) & \sqrt{\varepsilon_2/\varepsilon_{\rm h}}\, y_n(k_2r_2) & h_n^{(1)}(k_{\rm h}r_2) \\ 0 & \sqrt{\varepsilon_{\rm h}/\varepsilon_2}\, u_n'(k_2r_2) & \sqrt{\varepsilon_{\rm h}/\varepsilon_2}\, v_n'(k_2r_2) & w_n'(k_{\rm h}r_2) \end{vmatrix}. \tag{8}$$

The general formulas (4)–(8) are in agreement with the previously obtained expressions [30,33,34], which provide the final result for the expansion coefficients of the TM- and TE-modes for two-layered spherical particles.

3. Simple Formulas of the Quasistatic Approximation

Here we consider the case of particles whose overall radius is much smaller than the wavelength of light. Then one can use the quasistatic approximation of the Mie theory, which corresponds to the well-known results of the Rayleigh theory. In this case, the cross sections of absorption $\sigma_{\rm abs}$ and scattering $\sigma_{\rm scat}$ of light by a particle are given by

$$\sigma_{\rm abs}(\omega) = 4\pi k_{\rm h} V \,{\rm Im}\left\{\widetilde{\alpha}(\omega)\right\}, \tag{9}$$

$$\sigma_{\rm scat}(\omega) = \frac{8\pi}{3} k_{\rm h}^4 V^2 \left|\widetilde{\alpha}(\omega)\right|^2. \tag{10}$$

Here, $k_{\rm h}$ is the wave number of light in the host medium, $\alpha = \widetilde{\alpha} V$ and V are the polarizability and overall volume of the particle, and $\widetilde{\alpha}$ is its polarizability per unit volume.

According to this model, the polarizability of a bare metallic particle with radius r and permittivity $\varepsilon = \varepsilon_{\rm m}$ can be written as [44]

$$\alpha(\omega) = V\widetilde{\alpha}(\omega), \qquad \widetilde{\alpha} = \frac{3}{4\pi}\frac{\varepsilon_{\rm m} - \varepsilon_{\rm h}}{\varepsilon_{\rm m} + 2\varepsilon_{\rm h}}, \tag{11}$$

where $\varepsilon_{\rm h}$ is the permittivity of the host medium and $V = 4\pi r^3/3$.

Thus, the absorption and scattering cross sections are reduced to the particularly simple forms

$$\sigma_{\rm abs} = 4\pi k_{\rm h} r^3 \,{\rm Im}\left\{\frac{\varepsilon_{\rm m} - \varepsilon_{\rm h}}{\varepsilon_{\rm m} + 2\varepsilon_{\rm h}}\right\} = \frac{12\,\pi k_{\rm h} r^3\,{\rm Im}\{\varepsilon_{\rm m}/\varepsilon_{\rm h}\}}{\left({\rm Re}\{\varepsilon_{\rm m}/\varepsilon_{\rm h}\} + 2\right)^2 + \left({\rm Im}\{\varepsilon_{\rm m}/\varepsilon_{\rm h}\}\right)^2}, \tag{12}$$

$$\sigma_{\rm scat} = \frac{8\pi}{3} k_{\rm h}^4 r^6 \left|\frac{\varepsilon_{\rm m} - \varepsilon_{\rm h}}{\varepsilon_{\rm m} + 2\varepsilon_{\rm h}}\right|^2. \tag{13}$$

Note that, in the small particle limit ($k_{\rm h} r \ll 1$), the value of the scattering cross section $\sigma_{\rm scat}$ is much smaller than the absorption cross section $\sigma_{\rm abs}$.

The effective permittivity $\varepsilon_2^{\rm eff}$ of the core–shell spherical particle, which is equivalent to the permittivity of the homogeneous particle, is given by (see, e.g., [38])

$$\varepsilon_2^{\rm eff} = \frac{\varepsilon_2}{\varepsilon_{\rm h}} \frac{2\left(1 - (r_1/r_2)^3\right) + \left(1 + 2\,(r_1/r_2)^3\right)(\varepsilon_1/\varepsilon_2)}{\left(2 + (r_1/r_2)^3\right) + \left(1 - (r_1/r_2)^3\right)(\varepsilon_1/\varepsilon_2)}. \tag{14}$$

Here, r_1 and r_2 are the inner and outer radii of the concentric spheres, and $\varepsilon_1 = \varepsilon_{\rm m}$, $\varepsilon_2 = \varepsilon_{\rm J}$, and $\varepsilon_{\rm h}$ are the dielectric functions of the metallic core, J-aggregate shell, and a host medium, respectively. Thus, in the small-particle limit, the polarizability α of a concentric two-layered sphere with overall volume V can be written as

$$\alpha = V\widetilde{\alpha}, \quad V = \frac{4\pi r_2^2}{3}, \quad \widetilde{\alpha} = \frac{3}{4\pi} \frac{(\varepsilon_1 - \varepsilon_2)(2\varepsilon_2 + \varepsilon_{\rm h})(r_1/r_2)^3 + (\varepsilon_2 - \varepsilon_{\rm h})(2\varepsilon_2 + \varepsilon_1)}{2(\varepsilon_1 - \varepsilon_2)(\varepsilon_2 - \varepsilon_{\rm h})(r_1/r_2)^3 + (\varepsilon_2 + 2\varepsilon_{\rm h})(2\varepsilon_2 + \varepsilon_1)}. \tag{15}$$

This expression combined with Eqs. (9) and (10) allows us to evaluate analytically the electric-dipole contribution to the absorption and scattering cross sections by two-layered particles in the quasistatic approximation.

4. Dielectric Functions

The local dielectric function of a noble metal can be presented as the sum of the intraband transitions and interband transitions

$$\varepsilon(\omega) = \varepsilon_{\rm intra}(\omega) + \varepsilon_{\rm inter}(\omega). \tag{16}$$

The first term in (16) corresponds to the electronic response of free electrons in the conduction band and can be described by a Drude-like expression

$$\varepsilon_{\rm intra}(\omega) = \varepsilon_{\rm m}^{\infty} - \frac{\omega_{\rm p}^2}{\omega^2 + i\omega\gamma_{\rm intra}}. \tag{17}$$

Here, $\omega_{\rm p}$ is the effective plasma frequency, $\gamma_{\rm intra}$ is the effective plasma damping constant, ($1/\gamma_{\rm intra}$ is the corresponding decay time), and $\varepsilon_{\rm m}^{\infty}$ is the high frequency component of the metal dielectric function.

In the present work, the contribution of intraband transitions to the frequency-dependent dielectric function of the metallic core is described, taking into account the size effect associated with the scattering of free electrons from the metal/dielectric interface of the nanoparticle. It becomes particularly important when the particle radius is considerably smaller than the mean free path of electrons l_{∞} in the bulk metal [44, 45]. In such a situation, it is necessary to take into account the dependence of the effective plasma damping constant $\gamma_{\rm intra}$ on the radius r_1 of the metallic core. Explicit expressions for size-dependent value of $\gamma_{\rm intra}$ can be derived within the framework of the quantum description of the confined electronic states in a sphere [46]. We use here the phenomenological expression [44, 45] for the effective damping constant

$$\gamma_{\rm intra}^{(r)} = \gamma_{\rm intra}^{\rm bulk} + \xi \frac{v_{\rm F}}{r_1}\,. \tag{18}$$

Here, $v_{\rm F}$ is the Fermi velocity, ξ is the dimensionless constant of the order of unity, whose magnitude should be determined from a comparison of the theory for a bare metallic particle with the experiment. When the particle size is much greater than the mean free path of electrons l_{∞} in the bulk matter, the damping constant in Eq. (17) becomes equal to its size-independent value $\gamma_{\rm intra}^{\rm bulk}$. However, when the core radius r_1 becomes smaller than l_{∞}, the value of $\gamma_{\rm intra}^{(r)}$ gives the required dependence of the scattering electron frequency on the particle size. A discussion of the effects associated with the size-dependent dielectric function of a metallic core in studies of the optical properties of different metal-based nanoparticles is also presented in [26, 27, 43, 47–49].

The second term in (16) corresponds to the electronic transitions between the d valence band and the sp conduction band. It is usually described within the framework of the random phase approximation [50, 51]

$$\varepsilon_{\rm inter}(\omega) = K \int\limits_{\omega_{\rm g}}^{\infty} dx \frac{\sqrt{x-\omega_{\rm g}}}{x} \left[1 - F(x,\Theta)\right] \frac{\left(x^2 - \omega^2 + \gamma_{\rm inter}^2 - 2i\omega\gamma_{\rm inter}\right)}{\left(x^2 - \omega^2 + \gamma_{\rm inter}^2\right)^2 + 4\omega^2\gamma_{\rm inter}^2}. \tag{19}$$

Here, $F(x,\Theta)$ is the energy distribution function of conduction electrons whose energy is $\hbar x$ at temperature Θ, and $\gamma_{\rm inter}$ represents the damping constant in the band-to-band transition. For the interband transitions, a dispersionless d band and a parabolic conduction sp band with minimum energy $\hbar\omega_g$ with respect to the d band is assumed. The constant K is determined by the oscillator strength of the interband transitions [51].

In contrast to the contribution of free electrons (17) to the total dielectric function of the metallic particle, the contribution of bound electrons (19) is slightly affected by the influence of the size-dependent effect. Therefore, to describe correctly both contributions (16) to the dielectric function of the metallic core taking into account the size-dependent effect, one can use the expression

$$\varepsilon_{\rm m}(\omega, r) = \varepsilon_{\rm bulk}(\omega) + \omega_p^2 \left(\frac{1}{\omega^2 + i\omega\gamma_{\rm intra}^{\rm bulk}} - \frac{1}{\omega^2 + i\omega\gamma_{\rm intra}^{(r)}} \right), \tag{20}$$

following the approach of [45]. Here, $\varepsilon_{\rm bulk}$ is the bulk permittivity of the metal obtained by fitting the experimental data [53] for Ag and Au, ω_p is the plasma frequency, $\gamma_{\rm intra}^{\rm bulk}$ is the scattering electron frequency in the bulk material, and $\gamma_{\rm intra}^{(r)}$ is the particle size-dependent scattering electron frequency determined from Eq. (18).

The dielectric function of the J-aggregate shell can be evaluated using the simple expression

$$\varepsilon_{\rm J}(\omega) = \varepsilon_{\rm J}^{\infty} + \frac{f\omega_0^2}{\omega_0^2 - \omega^2 - i\omega\Gamma} \ . \tag{21}$$

Here, we assume a Lorentzian shape of the absorption line of the molecular exciton J-band with specific parameters obtained from the experimental data, ω_0 is the transition frequency corresponding to the line center in the J-band, Γ is the line width, f is the reduced oscillator strength, and $\varepsilon_{\rm J}^{\infty}$ is the permittivity outside the J-band transition. For the cyanine dye J-aggregates under investigation, these parameters are presented in Table 4..

Table 1. Parameters of J-Aggregates of TC, OC, PIC, and NK2567 Cyanine Dyes Used in the Present Calculations.

J-aggregate	$\varepsilon_{\rm J}^{\infty}$	ω_0, eV	λ_0, nm	f	Γ, eV
TC	1	2.68	462.6	0.90	0.066
OC	1	3.04	407.2	0.01	0.039
PIC	2.9	2.13	582.1	0.10	0.033
NK2567	1	1.79	692.6	0.02	0.052

In this work, we study the optical properties of nanoparticles in aqueous solution. The dielectric function of water (the host medium) in the visible range can be found using the standard expressions $\mathrm{Re}\{\varepsilon_{\rm w}\} = n_{\rm w}^2 - \kappa_{\rm w}^2$ and $\mathrm{Im}\{\varepsilon_{\rm w}\} = 2n_{\rm w}\kappa_{\rm w}$ and reference data [52] for the refractive index $n_{\rm w}$. The very small imaginary part $\kappa_{\rm w}$ of the refractive index can be neglected. Note that the permittivity of water varies slowly in the whole visible range $\big(1.77 < \varepsilon_{\rm w} < 1.82$ at $350 < \lambda\ [\mathrm{nm}] < 700\big)$.

5. Main Features of the Absorption Spectra

Below we apply the general theory presented in Sec. 2 to the investigation of the extinction spectra of metallic nanoparticles (Ag, Au) covered with molecular J-aggregates of cyanine dyes (TC, OC, PIC, and NK2567). For such materials, the J-band absorption maxima are located in different wavelength ranges relative to the peak positions of surface plasmon resonances of noble metal particles in aqueous solutions, and the reduced oscillator strengths in the J-band strongly differ from each other (see Table 1). We performed our calculations for a wide range of wavelengths and geometrical parameters of the composite system, so that they cover both dipolar and quadrupolar scatterers. All these items allow us to demonstrate quite different shapes and the intensity distributions in the absorption and scattering spectra of metal/J-aggregate complexes.

In Fig. 2, we show our results for the absorption cross sections of the core-shell Ag/OC (panel a) and Au/TC (panel b) particles in aqueous solutions. The inner and outer radii of the concentric spheres are taken to be equal to $r_1 = 20$ nm and $r_2 = 23$ nm, respectively. The solid curves illustrate the typical spectral behavior of the photoabsorption processes for the hybrid noble metal/J-aggregate systems provided that the overall particle diameter is less than 50 nm. Then, in the visible range, there are two clearly pronounced peaks in the intensity distribution over the spectrum, which come from the dipolar localized surface plasmon resonance of the noble-metal core and the electronic excitation of the J-aggregated TC-dye coating. According to our results for the composite Ag/OC nanoparticles, such peaks in the absorption spectra appear at $\lambda_{\rm Ag}^{(1)} = 380$ nm and $\lambda_{\rm Ag}^{(2)} = 410$ nm, while for Au/OC nanoparticles the theory yields $\lambda_{\rm Au}^{(1)} = 410$ nm and $\lambda_{\rm Au}^{(2)} = 522$ nm.

Comparison of the results presented in Figs. 2 (panel a) and 2 (panel b) points to the distinctive features of the Ag/OC and Au/OC systems. In the case of Ag/OC particle, in the visible range there

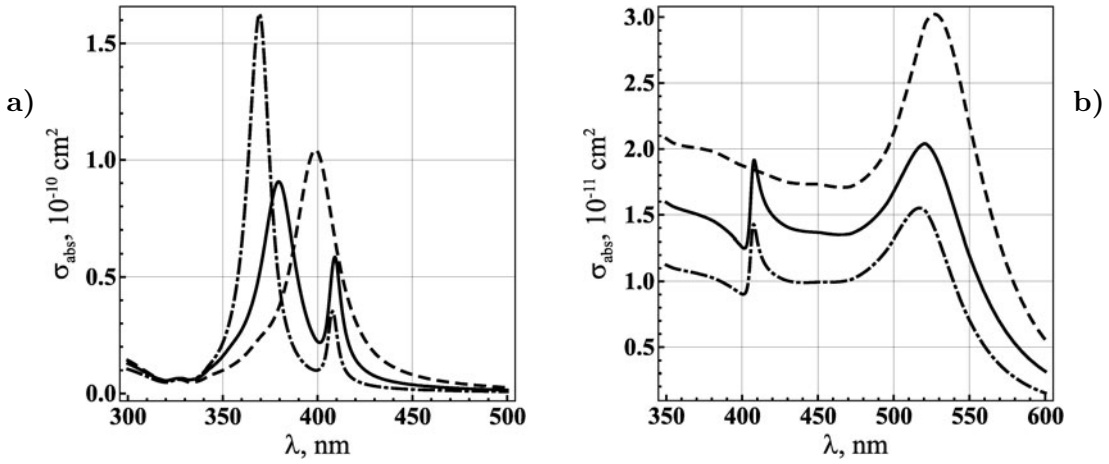

Fig. 2. Absorption cross sections $\sigma_{\rm abs}$ of Ag/OC (panel a) and Au/OC (panel b) particles in aqueous solution versus the light wavelength in vacuum λ (the core radius $r_1 = 20$ nm, the shell thickness $\ell = 3$ nm). The results obtained using the general Eqs. (1) and (4)–(8) combined with Eq. (21) for the permittivity of J-aggregate shell and the particle size-dependent permittivity (20) of the Ag core (solid curves). The corresponding results for the uncoated Ag- and Au-particles with $r = 20$ nm (dashed curves). The calculations made in the quasistatic approximation (9) using Eq. (15) for the dipole polarizability of the core–shell particle (dash-dotted curves).

are two absorption peaks differing substantially in intensities. The left peak is located close enough to the peak associated with the localized dipolar plasmon resonance in the uncoated silver particle. For a hybrid particle with core radius 20 nm and shell thickness 3 nm, the blue shift of this peak relative to the peak position of a bare Ag particle is equal to $\Delta\lambda = 19$ nm. This follows from the comparison of the solid and dashed curves in Fig. 2. Similarly, the right peak of a composite Ag/OC system exhibits a red shift relative to the unperturbed transition frequency ω_0 corresponding to the line center in the J-band of the OC dye. In the wavelength scale, it is equal to $\Delta\lambda = 3$ nm.

For the Au/OC particle, the right spectral peak of the composite system is blue shifted ($\Delta\lambda = 5$ nm) with respect to the peak position of the uncoated Au particle. The left peak turns out be red shifted ($\Delta\lambda = 3$ nm) with respect to the center of the line ($\lambda_{\rm OC} = 407$ nm) in the J band of the OC dye. This is a result of different connections between the excitation energies of the plasmon resonance and the Frenkel exciton in isolated Ag/OC and Au/OC systems. In the examples considered in Fig. 2, the absorption maximum of the J band for the OC dye ($\lambda_{\rm OC} = 407$ nm) is located between the peaks of the uncoated silver and gold particles with radius of 20 nm ($\lambda_{\rm Ag} = 399$ nm and $\lambda_{\rm Au} = 527$ nm, respectively).

In Fig. 3, we present the results of our calculations of the absorption cross sections for Ag/NK2567 (panel a) and Au/NK2567 (panel b) particles as functions of the light wavelength in vacuum. It is seen that, in the first case (panel a), the distinctions between the maximum intensities of the left and right peaks turn out to be particularly large due to the substantial difference $\Delta\lambda = \lambda_0^{(\rm J)} - \lambda_{\rm res}^{\rm Ag}$ in the positions of the plasmon-resonance peak of the uncoated silver nanoparticle and the line center of the NK2567-dye Jband ($\lambda_{\rm NK2567} = 693$ nm).

In the second case (panel b), both peaks are located closer to each other, and their maximum values are comparable. But the absolute value of the intensity of the right peak turns out to be approximately the same as in the case of Ag/NK2567 nanoparticle. This differs considerably from the case where the metallic core is covered with the OC J-aggregate. From Fig. 2, one can see that the material of the core significantly affects the maximum value of the exciton-peak intensity.

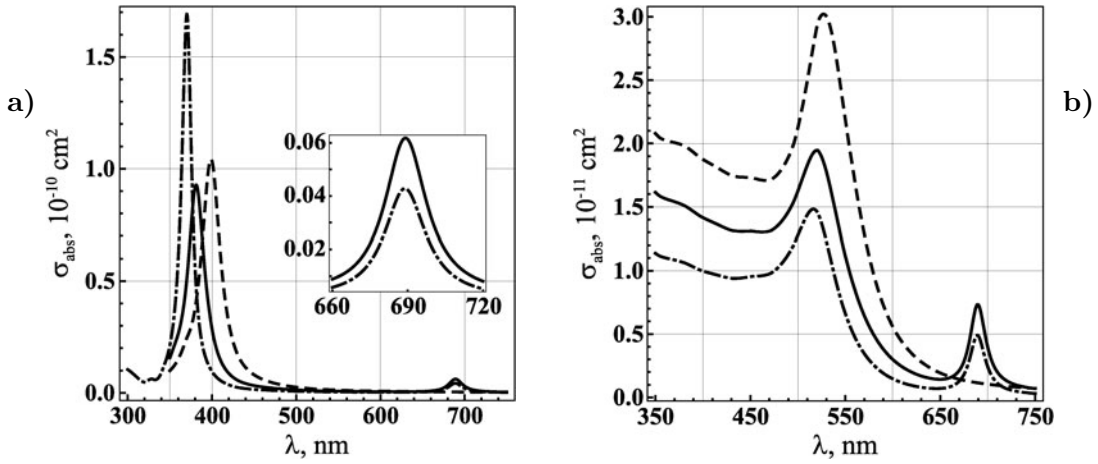

Fig. 3. Absorption cross sections $\sigma_{\rm abs}$ of the core-shell Ag/NK2567 (panel a) and Au/NK2567 (panel b) nanoparticles in aqueous solution versus light wavelength in vacuum λ (core radius $r_1 = 20$ nm, shell thickness $\ell = 3$ nm). The other notation is the same as in Fig. 2.

The calculations presented by the solid curves in Figs. 2 and 3 have been carried out using the general formulas (1), (4)–(8) of the extended Mie theory. The dash-dotted curves represent the corresponding results obtained in view of simple Eqs. (9) and (15) for the cross section of photoabsorption by the dipolar particles, which corresponds to the quasistatic approximation for the two-component spherical system. As is obvious from the comparison of the solid and dash-dotted curves, the quasistatic approximation allows one to explain qualitatively the presence of two peaks in the photoabsorption spectra. However, it is definitely inapplicable for a reliable quantitative description of the processes under consideration for the identified geometrical parameters of nanoparticles ($r_1 = 20$ nm, $\ell = 3$ nm). Thus, in this case, it is necessary to utilize the general formulas (1), (4)–(8) presented in Sec. 2.

The disagreements between the exact calculations of the absorption cross sections and those performed in the quasistatic approximation grow substantially with increase in the overall particle radius r_2. Furthermore, at large values of r_2, the quasistatic approximation is unable not only to provide reliable quantitative results, but also does not allow us to explain correctly some new features in the wavelength dependences of the absorption spectra. To demonstrate this fact, we show in Fig. 4 the results of our calculations of the absorption cross sections for hybrid Au/TC particles with core radius $r_1 = 42$ nm (panel a) and $r_1 = 55$ nm (panel b) and thickness of J-aggregate layer $\ell = 3$ nm.

One can see that even for an overall particle radius of $r_2 = 45$ nm (panel a), the behavior of the absorption cross section predicted by the general formulas differs substantially from that obtained using the simple formula of the quasistatic approximation, particularly, in the spectral range between 350 and 450 nm. This appears to be due to the presence of the quadrupolar plasmon resonance in the gold core of a hybrid particle perturbed by its interaction with the Frenkel exciton in the J-aggregated shell. A further increase in the particle radius leads to a significant change in the behavior of the absorption cross section. In particular, a substantial redistribution occurs in the peak intensities over the spectrum. This follows from our calculations presented in Fig. 4 b for the Au-core radius $r_1 = 55$ nm and the TC-dye shell of thickness 3 nm. For such particle radius, the difference in the behavior and the values of the absorption cross sections predicted by the extended Mie theory and the quasistatic approximation grows substantially. This is the result of an increase in the contribution of multipolar plasmon-supported modes interacting with the Frenkel exciton in a J-aggregated shell with increase in the core radius.

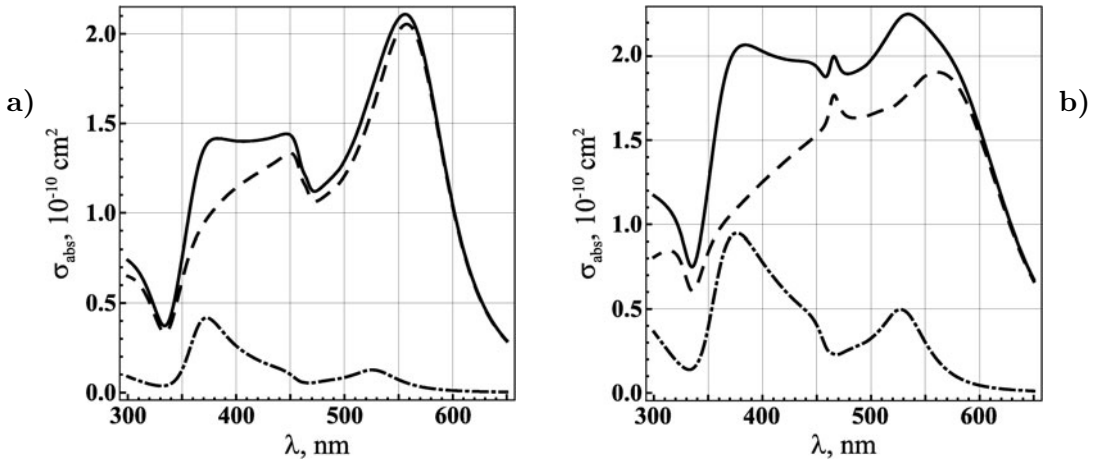

Fig. 4. Absorption cross sections $\sigma_{\rm abs}$ of Au/TC particles in aqueous solution versus the light wavelength in vacuum λ for the geometrical parameters: $r_1 = 42$ nm and $r_2 = 45$ nm (panel a), and $r_1 = 55$ nm and $r_2 = 58$ nm (panel b). The results obtained using general Eqs. (1) and (4)–(8) for the total contribution of all TM- and TE-modes (solid curves). The contributions of the dipolar $n = 1$ (dashed curves) and quadrupolar $n = 2$ (dash-dotted curves) terms in Eq. (1).

6. Comparison of Absorption and Scattering Cross Sections

We consider now the relative contribution of light scattering and absorption processes to the total extinction cross section in dependence on the size of the composite metal-organic nanoparticle. We carried out our calculations not only using the general formulas of the extended Mie theory for the Au-core and J-aggregated shell of the PIC dye. They cover three various sets of geometrical parameters of the core-shell particle (see Fig. 5). It is seen that in the visible range the scattering spectra consist of two main peaks if the size of the hybrid particle is not too large. Note also that the long-wavelength peak is split into two components. As follows from Fig. 5 a, the contribution of light scattering process to the total extinction cross section is sufficiently small compared to the photoabsorption process, provided that the particle radius is less than 25 nm.

An increase in the overall particle radius leads to a rapid growth of the scattering cross section. It directly follows from the comparison of simple formulas (9) and (10) of the quasistatic approximation, according to which $\sigma_{\rm abs} \propto r^3$ and $\sigma_{\rm scat} \propto r^6$. As a result, when the radius of the composite Au/PIC particle increases up to about 45 nm, the contribution of the scattering process becomes comparable with the photoabsorption (see the dash-dotted and dashed curves in Fig. 5 b), and further on it appears predominant. Finally, Fig. 5 c demonstrates the typical wavelength dependence of the extinction cross section under the condition of appreciable domination of light scattering process over the photoabsorption.

7. Size-Dependent Effects

All calculations presented above were carried out using the dielectric function of a noble metal core taking into account the size-dependent effect associated with scattering of free electrons on the metal–dye interface of a nanoparticle. However, this effect becomes especially strong when the particle size is considerably smaller than the mean free path of electrons l_∞ in the bulk silver or gold samples (l_∞ is equal

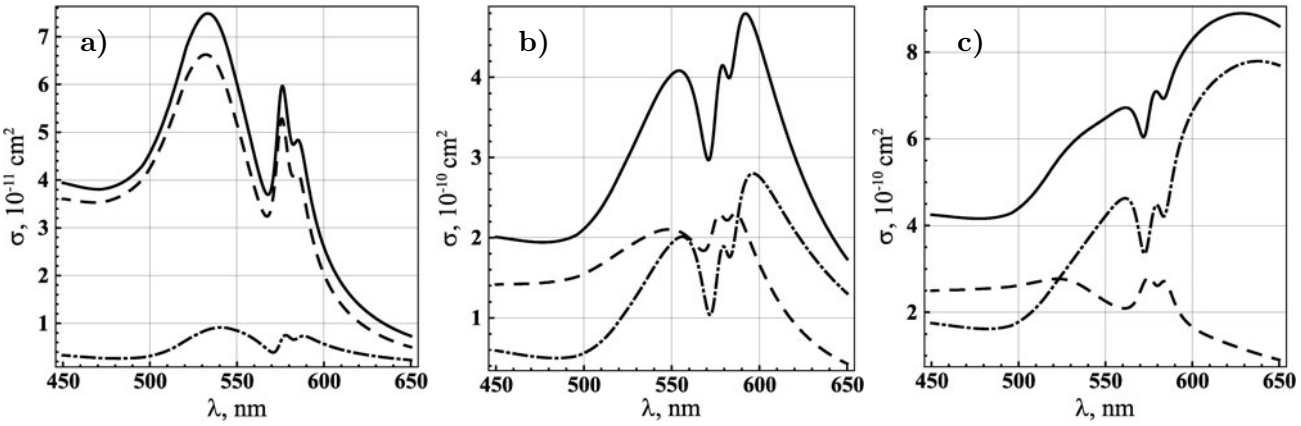

Fig. 5. Cross sections of extinction $\sigma_{\rm ext}$ (solid curves), absorption $\sigma_{\rm abs}$ (dashed curves), and scattering $\sigma_{\rm scat}$ (dash-dotted curves) of light by Au/PIC nanoparticles in aqueous solution. Calculations were performed for the following geometrical parameters: $r_1 = 25$ nm and $r_2 = 27$ nm (panel a), $r_1 = 45$ nm and $r_2 = 49$ nm (panel b), and $r_1 = 65$ nm and $r_2 = 70$ nm (panel c).

to 52 and 13 nm for Ag and Au, respectively). The case of small particle sizes is of particular interest because most of the available experimental data on the spectroscopic properties of metal/J-aggregate complexes have been obtained for an overall particle diameter of the order of 10 nm and J-aggregate layer of thickness about 1 nm (see [20–27]).

Here, we demonstrate the behavior and typical values of the absorption cross section for such nanoparticles by presenting our results for the Ag/J-aggregate and Au/J-aggregate systems composed of the TC, OC, and PIC dyes (see Figs. 6 and 7). It is seen that, for all the systems under consideration, the absorption cross sections are about two orders of magnitude smaller than the cross sections presented in Figs. 2 and 3. This is due to a decrease in the particle size by about four times. The positions of maxima in the absorption spectra and the intensity distribution strongly depend on the specific magnitudes of the

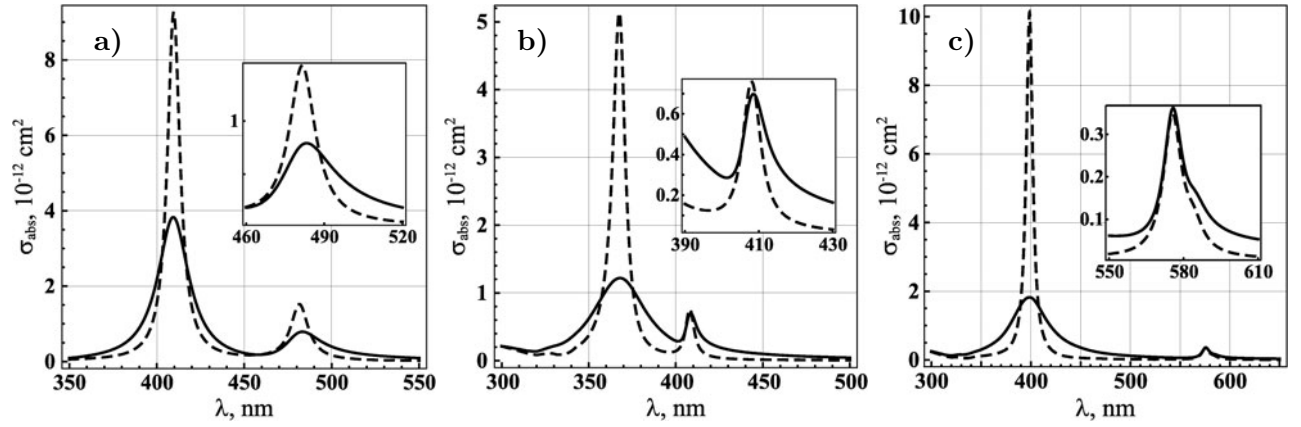

Fig. 6. Absorption cross sections $\sigma_{\rm abs}$ of Ag/TC (panel a), Ag/OC (panel b), and Ag/PIC (panel c) particles in aqueous solution versus the light wavelength in vacuum λ (core radius $r_1 = 5$ nm, shell thickness $\ell = 1$ nm). The results obtained using the permittivity (21) of the J-aggregate shell and size-dependent permittivity (20) of the Ag core (solid curves), and the same calculations obtained using the reference data [53] for the permittivity of bulk Ag (dashed curves).

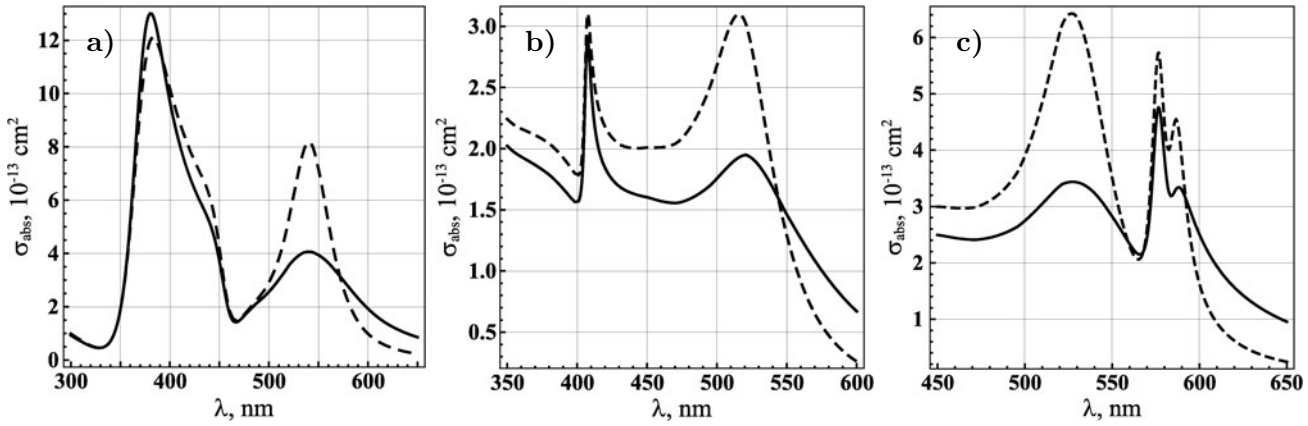

Fig. 7. Absorption cross sections $\sigma_{\rm abs}$ of Au/TC (panel a), Au/OC (panel b), and Au/PIC (panel c) particles in aqueous solution as functions of the light wavelength in vacuum λ (core radius $r_1 = 5$ nm, shell thickness $\ell = 1$ nm). The results obtained using the permittivity (21) of the J-aggregate shell and size-dependent permittivity (20) of the Au core (solid curves). The same calculations obtained using the reference data [53] for the permittivity of bulk Au (dashed curves).

optical constants of the core and shell materials and turn out to be quite different for Ag/J-aggregate and Au/J-aggregate complexes with TC, OC, and PIC dyes. Furthermore, as follows from the comparison of the solid and dashed curves in Figs. 6 and 7, the size-dependent effect (associated with scattering of free electrons on the metal–dye interface) significantly affects the absorption spectrum of a hybrid system in the whole visible range. However, its quantitative influence strongly depends on the optical constants of the core and shell materials and turns out to be different at various wavelength ranges.

For example, in the case of Ag/J-aggregate systems involving TC, OC, and PIC dyes (see Fig. 6), the use of the permittivity of bulk silver yields a considerably narrow width of the left peak as compared to the experimental data [20, 27]. At the same time, the use of the size-dependent permittivity of the Ag core [see Eqs. (18) and (20)] in calculations of the absorption cross sections of Ag/TC, Ag/OC, and Ag/PIC particles leads to widths of such a peak that are about 1.8, 4.0, and 5.6 times greater than those obtained using the permittivity of bulk Ag. Simultaneously, the intensities of these peaks decrease in their maxima by 2.4, 4.2, and 5.7 times, respectively. The inclusion of the size-dependent dielectric function of the silver core in the calculations is also important for the correct evaluation of the absorption-spectrum behavior in the wavelength range far from the left peak. In fact, as can be seen from Fig. 6, in spite of the fact that the influence of the size effect on the maximum intensity of the right peak is not as strong as in the case of the left peak, nevertheless, it appreciably affects the light-intensity distribution in this spectral range. This is particularly important in the cases of Ag/TC and Ag/OC systems because for Ag/PIC particles the plasmon–exciton coupling is sufficiently weak (see insets in Fig. 6).

We consider now the influence of the particle size in Eqs. (18) and (20) for the dielectric function of the gold core on the absorption spectrum of the Au/J-aggregate particles in aqueous solution. As directly follows from Fig. 7, the size effect particularly affects the values and the behavior of the absorption cross sections in the wavelength range between 500 and $550 - 600$ nm. For example, the peak intensities for Au/TC, Au/OC, and Au/PIC nanoparticles obtained using the size-dependent dielectric function $\varepsilon_{\rm Au}(\omega, r_1)$ of the gold core are about 2.0, 1.6, and 1.9 times lower than those obtained using the permittivity of the bulk Au sample. It is worthwhile to point out, however, that, on the whole, the overall influence of the size-dependent effect on the spectroscopic properties of Au/J-aggregate particles is some-

what weaker as compared to the case of Ag/J-aggregate systems. This is due to the fact that, in the range of $\hbar\omega \lesssim 3.5$ eV, the main contribution to the permittivity of silver comes from free electrons while, in the case of the gold core, bound electrons also play a significant role starting from $\hbar\omega \gtrsim 1.7$ eV. Moreover, the electron mean free path for gold ($l_\infty^{\mathrm{Au}} = 13$ nm) is much shorter than that for silver ($l_\infty^{\mathrm{Ag}} = 52$ nm). Correspondingly, at a particle size from 5 to 10 nm, the increase in the electron scattering frequency induced by collisions with the particle surface has a much weaker effect on the dielectric properties of gold nanoparticles.

The influence of geometrical parameters of a composite particle on the spectral behavior of the absorption and scattering processes is not only a result of the dependence of the effective plasma damping constant γ_{intra} on the core radius that leads to the size-dependent dielectric function $\varepsilon_{\mathrm{intra}}$ of a metallic core. As directly follows from the simple formulas of the quasistatic approximation (9), (10), and (15), the polarizability α of a hybrid particle and the cross sections σ_{abs} and σ_{scat} strongly depend on the dielectric properties of its core and shell materials, as well as on the overall radius r_2 and the ratio r_1/r_2 of internal and external radii of concentric spheres. Moreover, an increase in the overall particle size leads to more complicated dependences of the optical spectra on geometrical parameters of a metal-organic system than those predicted by simple limiting expressions of the quasistatic approximation.

Below we present some additional calculations, which clearly demonstrate significant changes in positions and intensities of spectral peaks in photoabsorption even at rather small changes in the geometrical parameters of the metal/J-aggregate nanoparticle (see Fig. 8). We performed our analysis for two different cases: (i) for particles with constant size of the Ag-core ($r_1 = 10$ nm) and thickness $\ell = r_2 - r_1$ of the J-aggregate shell of the OC dye varied from 1 up to 5 nm (panel a); (ii) for particles of the same composition with fixed thickness of their shell ($\ell = 3$ nm) and core radius r_1 varied from 8 up to 12 nm (panel b).

We note that the intensities and mutual positions of both peaks strongly depend on the ratio of the shell thickness $\ell = r_2 - r_1$ with respect to the radius of the composite particle. More precisely, the increase in ℓ with fixed value of r_1 leads to a significant shift of the left peak towards lower wavelengths (see Fig. 8 a) and to a decrease in its maximum. On the contrary, the increase in core radius r_1 with fixed value of ℓ leads to the shift of the left peak towards higher wavelengths (see Fig. 8 b), and its magnitude also grows. Note that in the first case (panel a) the ratio r_1/r_2 of the internal and external radii of the concentric spheres decreases from 0.91 to 0.67, while in the second case (panel b) it grows from 0.73 to 0.8. This explains the opposite behavior of the left spectral peak of a composite particle in the examples presented in Figs. 8 a and b. As for the second peak (the right one in Fig. 8), its position also changes with variation in the r_1/r_2 ratio, but very slightly. This absorption maximum shifts towards higher wavelengths in the first case (panel a) and in the opposite direction in the second case (panel b).

With increase in the particle size, the behavior of the absorption spectra becomes more complicated (see Fig. 9). As above, here we present our results for two cases: (i) for particles with constant size of the Ag core ($r_1 = 30$ nm) and shell thickness ℓ varied from 2 up to 12 nm (panel a); (ii) for particles with fixed thickness of their shell ($\ell = 3$ nm) and core radius r_1 varied from 29 to 39 nm (panel b). The spectra of such nanoparticles differ from each other not only in the positions and intensities of the peaks but also in a number of maxima. For example, there are three absorption peaks in the visible range and an additional peak with low intensity in the UV-range ($\lambda_{\max} \sim 320 - 330$ nm) for the Ag/OC-particle with core radius $r_1 = 30$ nm and shell thickness $\ell = 12$ nm (see curve 6 in Fig. 9 a). At the same time, for such a particle with internal radius $r_1 = 39$ nm and $\ell = 3$ nm, there are only two maxima in the visible range and one maximum in the UV range (see curve 6 in Fig. 9 b). These differences in spectral behavior

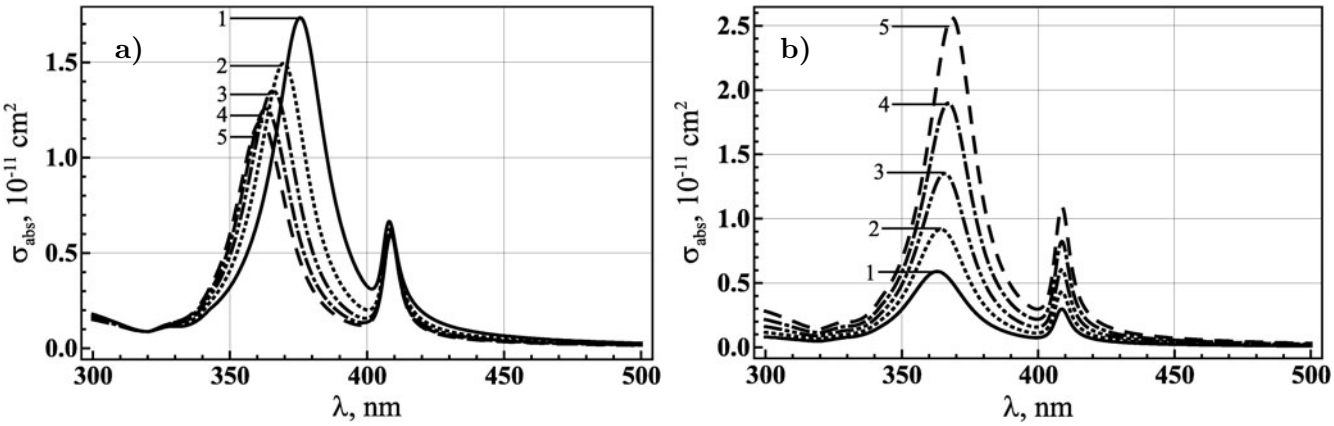

Fig. 8. Absorption cross sections of Ag/OC particles in aqueous solution versus the light wavelength in vacuum. The results obtained for the fixed core radius $r_1 = 10$ nm and various shell thickness $\ell = 1$ nm (1), 2 nm (2), 3 nm (3), 4 nm (4), and 5 nm (5) (panel a). The calculations for the fixed shell thickness $\ell = 3$ nm and various core radius 8 nm (1), 9 nm (2), 10 nm (3), 11 nm (4), and 12 nm (5) (panel b).

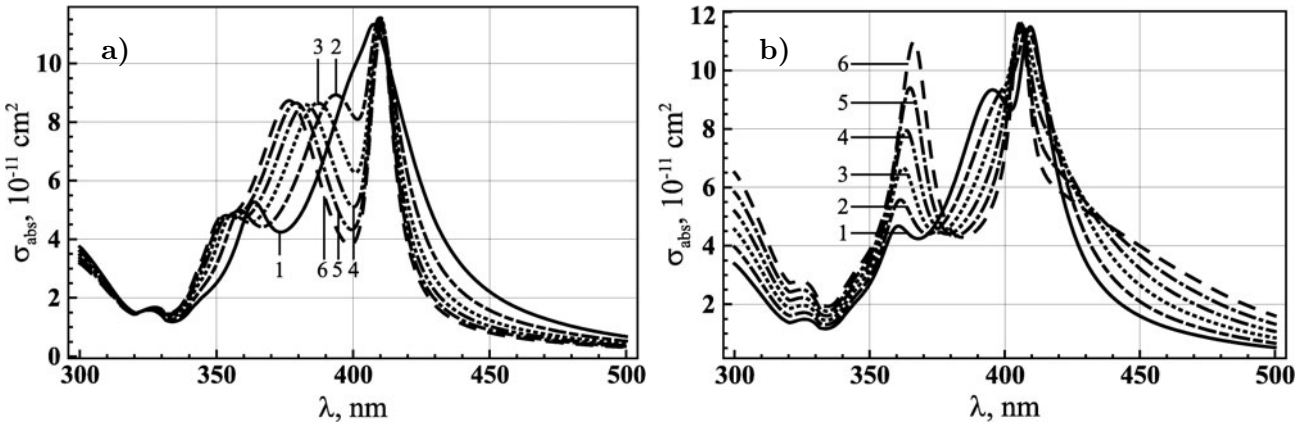

Fig. 9. Absorption cross sections of Ag/OC particles in aqueous solution versus the light wavelength in vacuum. The results obtained for a fixed value $r_1 = 30$ nm of the core radius and various shell thickness $\ell = 2$ nm (1), 4 nm (2), 6 nm (3), 8 nm (4), 10 nm (5), and 12 nm (6) (panel a). The calculations for the fixed shell thickness $\ell = 3$ nm and various core radius 29 nm (1), 31 nm (2), 33 nm (3), 35 nm (4), 37 nm (5), and 39 nm (6) (panel b).

take place despite the fact that the external particle radii $r_2 = 42$ nm are equal to each other in both cases. Note that the peak in the vicinity of $\lambda \sim 360 - 370$ nm is the result of the quadrupole plasmon resonance in the metallic core perturbed by its interaction with the Frenkel exciton in the J-aggregate shell. One more important feature consists in the behavior of the peaks resulting from the coupling of the exciton with the dipolar plasmon. It is seen in Fig. 9 b that with increase in the core radius, the middle and right peaks in the visible range are shifted towards each other and finally form a single absorption maximum near 406 nm.

8. The Influence of the Oscillator Strength on the Absorption Spectra of Hybrid Nanoparticles

We consider here the influence of the reduced oscillator strength f in the molecular J band of a dye shell on the positions of maxima and the peak intensities in the absorption spectra of Ag/J-aggregate

and Au/J-aggregate particles (see Figs. 10 and 11). Except for the oscillator strength, all other optical constants related to the J-aggregate shell are taken the same as in the case of the OC and TC dyes (see Table 1).

Since the core radius in the calculations presented in Figs. 10 a and 11 a does not exceed 20 nm, the high-order multipole resonances (quadrupole and others) do not make a significant contribution to the absorption cross section. Hence the hybrid modes in a composite system appear only as a result of the interaction between the Frenkel exciton in the OC- or TC-dye shell with the dipolar plasmon resonance in the Ag or Au core. Therefore, it is not surprising that at $f \neq 0$ the absorption spectrum of the Ag/J-aggregate system consists of three different peaks in accordance with our analytical model developed in [43].

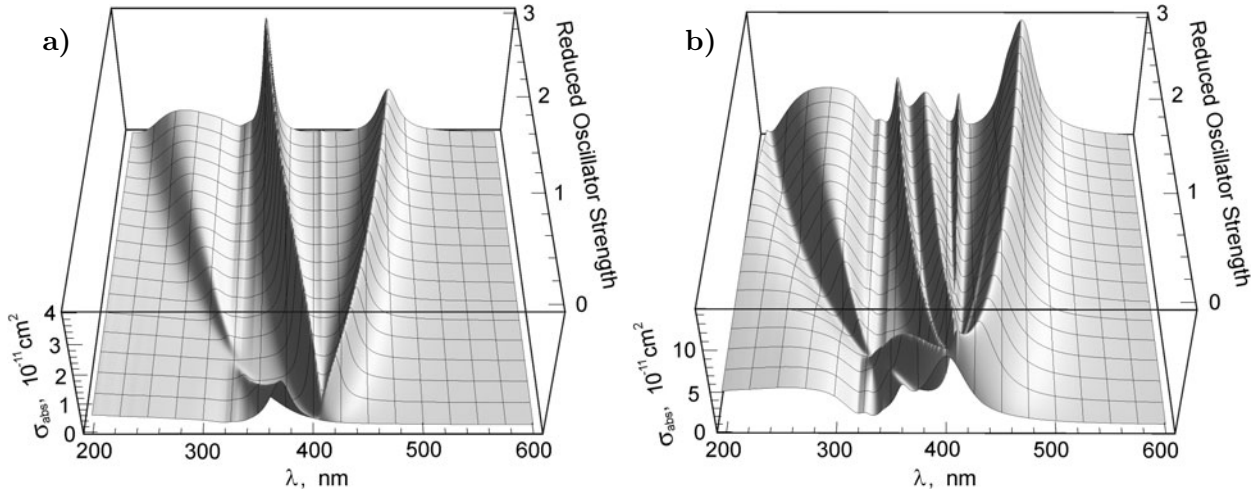

Fig. 10. Cross section of the light absorption by Ag/J-aggregate nanoparticles in aqueous solution as a function of the light wavelength in vacuum λ and the reduced oscillator strength f in the molecular J-band. The core radii and shell thickness are $r_1 = 10$ nm and $r_2 - r_1 = 2$ nm (panel a) and $r_1 = 30$ nm and $r_2 - r_1 = 3$ nm (panel b).

It is seen from Fig. 10 a that these peaks behave in a different manner with change in the oscillator strength. An increase in f leads to a shift in the position of the maximum of the "long-wavelength" peak towards large wavelengths. Simultaneously the positions of maxima of the "middle-wavelength" and "short-wavelength" peaks exhibit shifts towards small wavelengths. When $f \to 0$, the "long-wavelength" and "middle-wavelength" peaks move towards each other, forming a uniform peak. The corresponding maximum value of the absorption cross section tends to zero with decreasing f. At the same time, the frequency of the "short-wavelength" peak falls with decrease in the f value and becomes $\hbar\omega \approx 3.34$ eV at $f = 0$ for specific magnitudes of the core radius and shell thickness chosen in our calculations (see Fig. 10 a). The intensity of this peak is not equal to zero at $f \to 0$. Therefore, the absorption spectrum at $f = 0$ consists of only one peak. This corresponds to the limiting case of a silver particle coated by a thin dielectric layer with a constant permittivity $\varepsilon_{\mathrm{J}}^{\infty}$ and surrounded by a host medium (water in our calculations) with permittivity ε_{w}.

As we have already pointed out, the intensities of "long-wavelength" and "middle-wavelength" spectral peaks are equal to zero at $f \to 0$. As is obvious from Fig. 10 , the intensities of both peaks grow with increase in the f value in the whole range of f under consideration. At the same time, the intensity of the "short-wavelength" peak first falls with increase in the oscillator strength, and then becomes equal

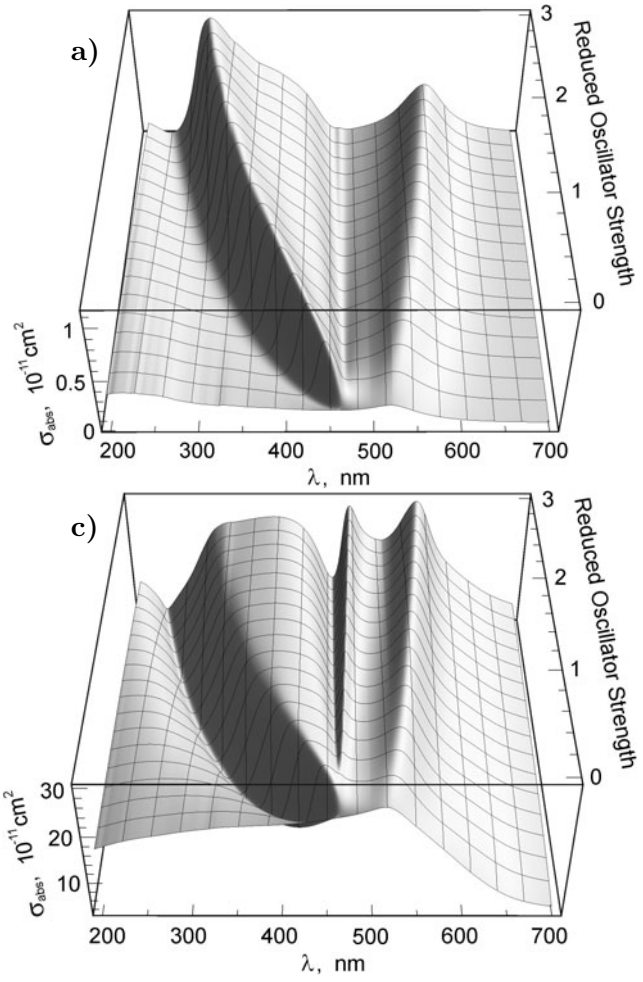

Fig. 11. Cross section of the light absorption by Au/J-aggregate nanoparticles in aqueous solution as a function of the light wavelength in vacuum λ and the reduced oscillator strength f in the molecular J band. The core radii and shell thickness are $r_1 = 10$ nm and $r_2 - r_1 = 2$ nm (panel a), $r_1 = 30$ nm and $r_2 - r_1 = 3$ nm (panel b), and $r_1 = 65$ nm and $r_2 - r_1 = 5$ nm (panel c).

to zero at $f \approx 0.6$. The further increase in the value of f leads to a growth in the intensity of the "short-wavelength" peak. Notice that the dip in the behavior of the cross-section maximum can be easily explained, in view of Eqs. (9) and (15) of the quasistatic approximation.

The other behavior of the absorption cross section as a function of the wavelength and oscillator strength occurs for Au/J-aggregate particles in aqueous solution (see Fig. 11 a). When $f = 0$, the absorption spectrum has a single peak, corresponding to the plasmon resonance in a homogeneous gold particle coated by a dielectric layer with a constant permittivity $\varepsilon_{\mathrm{J}}^{\infty}$ and surrounded by a host medium with permittivity ε_{w}. This is similar to the case of a hybrid nanoparticle with a silver core. However, an increase in the reduced oscillator strength f leads to the appearance of a single additional absorption peak possessing sufficiently large width. The position of the maximum of this peak is shifted towards small wavelengths with a rise in the f value, while its width grows substantially.

As to the "long-wavelength" absorption maximum, its intensity also grows with increase in f, but its position turns out to be shifted in the opposite direction, i.e., towards large wavelengths.

We obtained the results presented in Figs. 10 a and 11 a for sufficiently small overall size of a composite particle ($r_1 = 10$ nm and $r_2 = 12$ nm), when the spectral behavior is determined by the interaction of the Frenkel exciton with the dipolar plasmon in a metallic core. With a considerable increase in the particle

radius, the Frenkel exciton interacts with both the dipole and quadrupole plasmons in the metallic core. In the case of Ag/J-aggregate nanoparticle, this gives rise to some additional peaks in the absorption spectra of hybrid nanoparticles. We illustrate this feature in Fig. 10 b, where we present the results of our calculations of the absorption cross section as a function of the wavelength and oscillator strength performed for internal particle radius $r_1 = 30$ nm and J-aggregate shell thickness $\ell = r_2 - r_1 = 3$ nm.

For the composite Au/J-aggregate system, an increase in the overall particle radius leads to a considerable redistribution of the intensity over the spectrum in addition to the usual growth in the magnitudes of the absorption cross sections (see Fig. 11 b). Moreover, the width of the "short-wavelength" spectral peak grows so large that becomes more like a plateau for geometrical parameters of the composite system $r_1 = 30$ nm and $r_2 = 33$ nm, in particular, at large values of the reduced oscillator strength $f \gtrsim 1.5$. A further increase in the overall radius of the composite nanoparticle leads to the appearance of some new absorption peak (see Fig. 11 c). It is located between the "plateau" and the "long-wavelength" maximum. Additional spectral peaks appear here only at sufficiently large values of r. All this indicates somewhat different features in the electromagnetic coupling between the localized plasmons and the Frenkel excitons in hybrid metal/J-aggregate complexes containing silver and gold as a metallic core.

9. Summary

To summarize, we have carried out a series of calculations of photoabsorption and scattering cross sections for noble-metal nanoparticles covered with different cyanine dyes. We showed that, depending on geometrical parameters and optical constants of the core and shell materials, the total number of peaks in the extinction spectra can be variable and their intensities can be close to each other or strongly differ in magnitudes (see Figs. 5–9). This is a result of the quite different influence of the plasmon–exciton interaction in such hybrid complexes.

We paid special attention in this work to a detailed investigation of size effects. At small values of the overall particle radius, the absorption cross section of metal/J-aggregate complexes is determined by the contribution of the electric-dipole term and can be reasonably described in the quasistatic approximation. In this range, the contribution of scattering processes to the extinction cross section is small (see Fig. 5a). The simple formulas (9) and (15) of the quasistatic approximation become inapplicable for a reliable quantitative description of the absorption process when the particle radius is greater than $\sim 10 - 15$ nm. With further increase in the particle size, the absorption cross sections exhibit a more complicated spectral behavior due to the influence of additional multipolar plasmon-supported modes.

Some features in the extinction spectra result from the competition of contributions of the absorption and scattering processes with increase in particle size. For silver particles covered with J-aggregates, the total extinction cross section is primarily determined by the absorption process for radii less than $25 - 35$ nm, depending on the specific values of λ and the shell thickness. The contribution of the scattering process becomes predominant for greater values of the particle radius. For hybrid particles with a gold core, the scattering process is predominant starting from values of $r_2 = 55 - 60$ nm.

Our calculations demonstrate that the peak positions in the absorption and scattering spectra strongly depend on the reduced oscillator strength f of the J band in a dye shell. The variation in f leads also to the significant redistribution of the peak intensities over the spectrum. Thus, the value of f strongly affects the plasmon–exciton coupling strength. All this indicates that there is a possibility of effective control of the plasmon–exciton interaction and optical properties of hybrid materials based on the metal-organic nanoparticles.

Acknowledgments

This work was supported by the Russian Foundation for Basic Research under Project No. 12-02-00713_a, the Russian Ministry of Education and Science under Agreements Nos. 8576 and 8396, and the Physical Sciences Division of the Russian Academy of Sciences under Programmes "Fundamental Optical Spectroscopy and its Applications" and "Fundamental Aspects of the Physics and Technology of Semiconductor Lasers as Cornerstones of Photonics and Quantum Electronics."

References

1. Y. Shirasaki, G. J. Supran, M. G. Bawendi, and V. Bulovic, *Nature Photonics*, **7**, 13 (2013).
2. L.-Y. Chang, R. R. Lunt, P. R. Brown, et al., *Nano Lett.*, **13**, 994 (2013).
3. T. Yatsui, S. Sangu, T. Kawazoe, et al., *Appl. Phys. Lett.*, **90**, 223110 (2007).
4. A. Agrawal, C. Susut, G. Stafford, et al., *Nano Lett.*, **11**, 2774 (2011).
5. B. C. Das and A. J. Pal, *Phil. Trans. R. Soc. A*, **367**, 4181 (2009).
6. M. Ohtsu (Ed.), *Nanophotonics and Nanofabrication*, Wiley-VCH, Wenheim (2009).
7. W. Cai and V. Shalaev, *Optical Metamaterials: Fundamentals and Applications*, Springer, New York (2010).
8. F. J. García-Vidal, L. Martín-Moreno, T. W. Ebbesen, and L. Kuiperes, *Rev. Mod. Phys.*, **82**, 729 (2010).
9. T. I. Kuznetsova and V. S. Lebedev, *Phys. Rev. B*, **70**, 035107 (2004).
10. T. I. Kuznetsova and V. S. Lebedev, *Phys. Rev. E*, **78**, 016607 (2008).
11. M. A. Noginov, G. Zhu, A. M. Belgrave, et al., *Nature*, **460**, 1110 (2009).
12. I. E. Protsenko, *Phys. Uspekhi*, **55** 1040 (2012) [*Usp. Fiz. Nauk*, **82**, 1116 (2012)].
13. M.-C. Daniel and D. Astruc, *Chem. Rev.*, **104**, 293 (2004).
14. C. Burda, X. Chen, R. Narayanan, and M. A. El-Sayed, *Chem. Rev.*, **105**, 1025 (2005).
15. F. J. Garcia de Abajo, *Rev. Mod. Phys.*, **79**, 1267 (2007).
16. M. Quinten, *Optical Properties of Nanoparticle Systems: Mie and beyond*, Wiley-VCH, Wenheim (2011).
17. S. J. Oldenburg, R. D. Averitt, S. L. Westcott, and N. J. Halas, *Chem. Phys. Lett.*, **288**, 243 (1998).
18. N. J. Halas, S. Lal, W.-S. Chang, et al., *Chem. Rev.*, **111**, 3913 (2011).
19. T. Kobayashi (Ed.), *J-Aggregates*, World Scientific, Singapore (1996).
20. N. Kometani, M. Tsubonishi, T. Fujita, et al., *Langmuir*, **17**, 578 (2001).
21. T. Sato, F. Tsugawa, T. Tomita, and M. Kawasaki, *Chem. Lett.*, **30**, 402 (2001).
22. J. Hranisavljevic, N. M. Dimitrijevic, G. A. Wurtz, and G. P. Wiederrecht, *J. Am. Chem. Soc.*, **124**, 4536 (2002).
23. G.A. Wurtz, J. Hranisavljevic, and G. P. Wiederrecht, *J. Microsc.*, **210**, 340 (2003).
24. G. P. Wiederrecht, G. A. Wurtz, and J. Hranisavljevic, *Nano Lett.*, **4**, 2121 (2004).
25. G. P. Wiederrecht, G. A. Wurtz, and A. Bouhelier, *Chem. Phys. Lett.*, **461**, 171 (2008).
26. V. S. Lebedev, A. G. Vitukhnovsky, A. Yoshida, et al., *Colloids Surfaces A: Physicochem. Eng. Aspects*, **326**, 204 (2008).
27. V. S. Lebedev, A. S. Medvedev, D. N. Vasil'ev, et al., *Quantum Electron.*, **40**, 246 (2010) [*Kvantovaya Élektron.*, **40**, 246 (2010)].
28. T. Uwada, R. Toyota, H. Masuhara, and T. Asahi, *J. Phys. Chem. C*, **111**, 1549 (2007).

29. D. D. Lekeufack, A. Brioude, A. W. Coleman, et al., *Appl. Phys. Lett.*, **96**, 253107 (2010).
30. A. L. Aden and M. Kerker, *J. Appl. Phys.*, **22**, 1242 (1951).
31. A. Güttler, *Ann. Phys. (Leipzig)*, **11**, 65 (1952).
32. G. Mie, *Ann. Phys.*, **25**, 377 (1908).
33. R. Ruppin and R. Englman, *J. Phys. Cond. Matt.*, **1**, 630 (1968).
34. K. A. Fuller, *Opt. Lett.*, **18**, 257 (1993).
35. R. Bhandari, *Appl. Opt.*, **24**, 1960 (1985).
36. Z. C. Wu and Y. P. Wang, *Radio Sci.*, **26**, 1393 (1991).
37. J. Sinzig and M. Quinten, *Appl. Phys. A*, **58**, 157 (1994).
38. A. Irimajiri, T. Hanai, and A. Inouye, *J. Theor. Biol.*, **78**, 251 (1979).
39. E. Prodan, P. Nordlander, and N. J. Halas, *Nano Lett.*, **3**, 1411 (2003).
40. N. G. Khlebtsov, *Quantum Electron.*, **38**, 504 (2008) [*Kvantovaya Élektron.*, **38**, 504 (2008)].
41. A. Alù and N. Engheta, *J. Opt. A: Pure Appl. Opt.*, **10**, 093002 (2008).
42. W. Qiu, B. G. DeLacy, S. G. Johnson, et al., *Opt. Exp.*, **20**, 18494 (2012).
43. V. S. Lebedev and A. S. Medvedev, *Quantum Electron.*, **42**, 701 (2012) [*Kvantovaya Élektron.*, **42**, 701 (2012)].
44. C. F. Bohren and D. R. Huffmann, *Absorption and Scattering of Light by Small Particles*, John Wiley & Sons, New York (1998).
45. U. Kreibig and M. Vollmer, *Optical Properties of Metal Clusters*, Springer, Berlin (1995).
46. R. Ruppin and H. Yatom, *Phys. Status Solidi B*, **74**, 647 (1976).
47. A. Moroz, *J. Phys. Chem. C*, **112** 10641 (2008).
48. B. N. Khlebtsov and N. G. Khlebtsov, *J. Biomed. Opt.*, **11**, 44002 (2006).
49. N. G. Khlebtsov, *J. Quant. Spectrosc. Radiat. Transf.*, **123**, 184 (2013).
50. D. Pines and P. Nozières, *The Theory of Quantum Liquids*, W.A. Benjamin, Inc., New York (1966), Vol. I.
51. J.-Y. Bigot, J.-C. Merle, O. Cregut, and A. Daunois, *Phys. Rev. Lett.*, **75**, 4702 (1995).
52. G. W. C. Kaye and T. H. Laby, *Tables of Physical and Chemical Constants and Some Mathematical Functions*, 16th ed., Longman (1995).
53. P. B. Johnson and R. W. Christy, *Phys. Rev. B*, **6**, 4370 (1972).